

Genome analysis

# MTTFsite: cross-cell type TF binding site prediction by using multi-task learning

Jiyun Zhou<sup>1,2</sup>, Qin Lu<sup>2</sup>, Lin Gui<sup>3</sup>, Ruifeng Xu<sup>1,\*</sup>, Yunfei Long<sup>2</sup> and Hongpeng Wang<sup>1</sup>

<sup>1</sup>School of Computer Science and Technology, Harbin Institute of Technology Shenzhen Graduate School, Shenzhen 518055, China, <sup>2</sup>Department of Computing, The Hong Kong Polytechnic University, Hung Hom 999077, Hong Kong and <sup>3</sup>Department of Computer Science, University of Warwick, Coventry CV4 4AL, UK

\*To whom correspondence should be addressed.

Associate Editor: Inanc Birol

Received on January 24, 2019; revised on May 19, 2019; editorial decision on May 23, 2019; accepted on May 30, 2019

## Abstract

**Motivation:** The prediction of transcription factor binding sites (TFBSs) is crucial for gene expression analysis. Supervised learning approaches for TFBS predictions require large amounts of labeled data. However, many TFs of certain cell types either do not have sufficient labeled data or do not have any labeled data.

**Results:** In this paper, a multi-task learning framework (called MTTFsite) is proposed to address the lack of labeled data problem by leveraging on labeled data available in cross-cell types. The proposed MTTFsite contains a shared CNN to learn common features for all cell types and a private CNN for each cell type to learn private features. The common features are aimed to help predicting TFBSs for all cell types especially those cell types that lack labeled data. MTTFsite is evaluated on 241 cell type TF pairs and compared with a baseline method without using any multi-task learning model and a fully shared multi-task model that uses only a shared CNN and do not use private CNNs. For cell types with insufficient labeled data, results show that MTTFsite performs better than the baseline method and the fully shared model on more than 89% pairs. For cell types without any labeled data, MTTFsite outperforms the baseline method and the fully shared model by more than 80 and 93% pairs, respectively. A novel gene expression prediction method (called TFChrome) using both MTTFsite and histone modification features is also presented. Results show that TFBSs predicted by MTTFsite alone can achieve good performance. When MTTFsite is combined with histone modification features, a significant 5.7% performance improvement is obtained.

**Availability and implementation:** The resource and executable code are freely available at <http://hlt.hitsz.edu.cn/MTTFsite/> and <http://www.hitsz-hlt.com:8080/MTTFsite/>.

**Contact:** [xuruifeng@hit.edu.cn](mailto:xuruifeng@hit.edu.cn)

**Supplementary information:** [Supplementary data](#) are available at *Bioinformatics* online.

## 1 Introduction

Transcription factor (TF)-binding sites (TFBSs) are important for understanding transcriptional regulatory networks and fundamental cellular processes, such as growth controls, cell-cycle progressions and developments, as well as differentiated cellular functions (Dror *et al.*, 2016; Wasserman and Sandelin, 2004; Zambelli *et al.*, 2013).

TFBSs are short and often degenerate sequence motifs (Bulyk, 2003), which makes them computationally difficult to predict at genomic scale. TFBSs can be represented by consensus sequences and position weight matrices (PWMs) (Stormo, 2000, 2013). The consensus sequence representation provides a convenient way for visual interpretation of TFBSs. But, nucleotide variations at each position make the consensus sequence representation unsuited to

represent TFBSs (Holloway et al., 2005; Lenhard et al., 2003). To overcome this problem, the PWM representation was proposed to represent TFBSs (Stormo, 2000, 2013). PWMs are derived from a set of aligned functionally related sequences and assume that the positions within each TFBS are independent of each other. However, some studies have shown that position dependencies do exist in TFBSs, such as crystal structure analyses (Luscombe et al., 2001), biochemical studies (Berger et al., 2006; Bulyk et al., 2002; Man and Stormo, 2001) and statistical analyses of large collections of TFBSs (Barash et al., 2003; Tomovic and Oakeley, 2007; Zhou and Liu, 2004). In order to integrate position dependencies in predictions, a new approach, called dinucleotide weight matrix (DWM), was proposed recently (Siddharthan, 2010). DWM extends PWM by taking into account dependencies between any two positions (Siddharthan, 2010). TFFM proposed by Mathelier and Wasserman (2013) further captures position dependencies for predictions. In TFFM, state transition probabilities in a hidden Markov model (HMM) (Marinescu et al., 2004) were used to model position dependencies. Although the above four representation methods can represent TFBSs, they capture only sequence features.

Recent approaches attempted to use histones modification features to improve the accuracy of TFBS predictions (Kumar and Bucher, 2016; Tsai et al., 2015; Won et al., 2010). Histone modification features refer to the post-translational modification levels of various histones in chromatin structures, which are closely related to the formation of TFBSs. Won et al. (2010) proposed an HMM-based method called Chromia by combined use of histone modification features and sequence features. Tsai et al. (2015) examined the contributions of sequence features, histone modification features and structure features in TFBS predictions (Breiman, 2001). They conclude that all these three feature types were significant in TFBS predictions.

Recent studies suggested that DNA shape features are another important type of features for TFBS predictions (Mathelier et al., 2016a). Mathelier et al. (2016a) proposed a method by using DNA shape features predicted by DNashape (Zhou et al., 2013) and achieved a very good prediction performance. Andrabi et al. (2017) proposed DynaSeq to predict molecular dynamics-derived ensembles of a more exhaustive set of DNA shape features and then used them to predict TFBSs. In addition to these DNA shape-based methods, several deep learning methods were proposed for TFBS predictions. DeepBind (Alipanahi et al., 2015), DeepSEA (Zhou and Troyanskaya, 2015) and DanQ (Quang and Xie, 2016) are three representative methods. DeepBind, proposed by Alipanahi, applies Convolutional Neural Network (CNN) to DNA sequence features. DeepSEA, proposed by Zhou and Troyanskaya, combines CNN and a multi-task learning method to learn representations. DanQ, an improved model of DeepSEA proposed by Quang and Xie, combines the use of CNN and recurrent neural network (RNN). All these three deep learning-based methods achieved very good predicting performance and are considered the state-of-the-art works.

When there exists large amount of labeled data, supervised computational methods can achieve very good performance. However, TFBSs for most TFs can only be identified by ChIP-Seq (Harbison et al., 2004; Iyer et al., 2001; Kim et al., 2005) or ChIP-chip (Ren et al., 2000), which are experimental techniques and are very labor-intensive and costly to run. TFs of many cell types do not have sufficient labeled data and some do not have any labeled data. It remains quite challenging to train predictors for TFs of cell types that lack labeled data. Nevertheless, several studies (Kumar and Bucher, 2016; Tsai et al., 2015; Won et al., 2010) have shown that TFBSs of a TF in different cell types have some common histone modification

features. A TF may also have common binding motifs in different cell types (Bryne et al., 2007; Matys et al., 2006). So computational methods can leverage on the labeled data available in other cell types to predict TFBSs for cell types lacking labeled data. In this paper, we propose a multi-task learning framework, called *MTTFsite*, for TFBS predictions. *MTTFsite* contains a shared CNN to learn common features for all cell types and a private CNN for each cell type to learn private features. When the target cell type has labeled data, its private features and the common features are combined to predict TFBSs. Thus, for a target cell type with labeled data, *MTTFsite* amounts to a *data augmentation method* due to the fact that labeled data in the target cell type is augmented by labeled data available in other cell types. When a target cell type does not have any labeled data, only the learned common features are used to predict TFBSs. Thus, for the target cell type without labeled data, the term *cross-cell type* refers to the fact that *MTTFsite* can use labeled data available in other cell types to learn common features by the shared CNN.

Gene expression predictions provide a foundation for understanding the transcriptional controls of cell identities, diseases and cell-based therapies. Many computational methods were proposed for gene expression predictions. DeepChrome (Singh et al., 2016), TEPI (Schmidt et al., 2017) and Zhang's method (Zhang and Li, 2017) are three state-of-the-art methods. DeepChrome (Singh et al., 2016) is a unified end-to-end architecture constructed by using CNN. The main advantage of DeepChrome is that it can capture both pairwise interactions between neighboring bins and between different histone modification features. However, DeepChrome does not use TFBSs of any TF in predictions. TEPI is a segmentation-based method that first predicts TFBSs by applying PWMs to open-chromatin regions (Schmidt et al., 2017) and then uses predicted TFBSs in gene expression predictions. Although TEPI can predict TFBSs by applying PWMs, only a small portion of TFs have known PWMs so far. Also, predicted TFBSs by PWMs usually have very high false positive rate due to the lack of position dependencies in PWM. Zhang's method combines 10 histone modification features, TFBSs of 15 TFs and one DNase-I hypersensitivity profile for gene expression predictions (Zhang and Li, 2017). As TFBSs of the 15 TFs are identified by experimental methods, this method is limited to only a very small number of cell types.

The objective of this work is to predict gene expressions for cell types without experimentally identified TFBSs for any TF. We propose a novel gene expression prediction method, referred to as *TFChrome*, by combined use of TFBSs predicted by *MTTFsite* and histone modification features. As *MTTFsite* can predict TFBSs for TFs in most cell types by leveraging on labeled data available in cross-cell types, *TFChrome* is capable of predicting gene expression for most cell types with or without labeled data.

## 2 Materials and methods

### 2.1 Datasets

TFs in five cell types, including GM12878, H1-hESC, HeLa-S3, HepG2 and K562, are used to evaluate our proposed method. As *MTTFsite* needs to be evaluated by TFs with labeled data in at least two cell types, where one is used for testing and the others for training, a total of 72 TFs are used to evaluate *MTTFsite*, where 17, 14, 18 and 23 TFs have labeled data in all the five cell types, four cell types, three cell types and two cell types, respectively. The available TFBSs of these TFs in these five cell types are identified by TF ChIP-seq experiments and their peaks can be downloaded from ENCODE (ENCODE Project Consortium, 2004) freely. The obtained peaks are usually provided in one of two formats: *narrow peak* and *broad peak*. Some TFs have well defined binding sites and can be modeled

by narrow peaks while binding sites of other TFs are less well localized and would better be modeled by broader peaks. So the narrow peak format is used if available. Otherwise, the broad peak format is used. Based on works by Alipanahi *et al.* (2015) and Zeng *et al.* (2016), the TFBS at each peak is defined as a 101-bp sequence by taking the midpoint of the peak as the center. Contrast to TFBSs, the non-TFBSs of a TF are defined as 101 bp DNA regions that cannot be bound by the target TF. Many works (Kumar and Bucher, 2016; Won *et al.*, 2010) used a shuffle method to construct non-TFBSs. In the shuffle method, a non-TFBS is constructed for each TFBS by shuffling the dinucleotides in the TFBS to keep the dinucleotide composition unchanged. In this study, however, as TFBSs need to be encoded by DNA sequences and histone modification features which need to be extracted from actual DNA sequences, we need to extract actual DNA fragments to construct non-TFBSs. So, we construct a non-TFBS for each TFBS by randomly selecting a 101-bp DNA fragment that has similar dinucleotide composition with the TFBS and is non-overlapping with all TFBSs. This way, we can construct the same number of non-TFBSs as TFBSs for each TF. For each TF in each cell type, the labeled data are divided into three separate, yet equal size folds: 1-fold for training, 1-fold for validation and 1-fold for test. The used TFs and its number of TFBSs in each cell types are listed in Supplementary Table S1, which also can be accessed freely from our web-server.

## 2.2 Feature representation

Two types of features are used to represent TFBSs: sequence features and histone modification features. *Sequence features* of a TFBS are represented by the one-hot vectors of all its 101 nucleotides. For a TFBS  $T_i$  with the middle point at the position  $i$  in a genome, the sequence features can be represented by a feature matrix of dimension of  $4 \times 101$  as follows:

$$S_{T_i} = [O(N_{i-50}), \dots, O(N_i), \dots, O(N_{i+50})] \quad (1)$$

where  $O(N_i)$  denotes the one-hot vector of nucleotide  $N_i$ . Seven types of *histone modification features* are used:  $H3K4me2$ ,  $H3K4me3$ ,  $H4K20me1$ ,  $H3K9ac$ ,  $H3K27ac$ ,  $H3K27me3$  and  $H3K36me3$  as they are available for all the five considered cell types. The ChIP-seq profiles for these histone modification features can be accessed freely from Kumar's work (Kumar and Bucher, 2016). Based on Won's work (Won *et al.*, 2010), we use the following scheme to apply histone modification features in MTTFsite: we first estimate the histone modification features for all non-overlapping 25-bp bins and then estimate the histone modification features for each 100-bp bin by averaging the four 25-bp bins within it. Finally, histone modification features of the twenty 100-bp bins around a putative TFBS are concatenated to represent it. So the histone modification features for a TFBS  $T_i$  can be represented as

$$C_{T_i} = [H(N_{i-999}, \dots, N_{i-898}), \dots, H(N_{i-99}, \dots, N_i), \dots, H(N_{i+901}, \dots, N_{i+1000})] \quad (2)$$

where  $H(\cdot)$  denotes the histone modification features for a 100-bp bin. Since we use seven histone modification features, the histone modification features of a TFBS can be represented by a feature matrix with dimension of  $7 \times 20$ .

## 2.3 Convolutional neural network

In recent years, CNN has been gradually introduced into bioinformatics to learn representations for protein sequences, DNA fragments and RNA fragments. For example, Alipanahi *et al.* (2015) developed DeepBind to predict binding sites for DNA- and

RNA-binding proteins by using CNN to learn representations for DNA fragments and RNA fragments. Wang *et al.* (2016) proposed a CNN-based method to learn representations for proteins in protein secondary structure predictions. As the actual TFBSs of a TF often contain specific binding motifs, CNN is suitable to learn representations for TFBSs.

## 2.4 Multi-task learning for TFBS prediction (MTTFsite)

Multi-task learning is an effective approach for improving the performance of a single task by leveraging on other related tasks (Liu *et al.*, 2017). Multi-task learning attempts to divide the features for multiple tasks into private and common features based on whether the features should be shared. Thus, in multi-task learning, each task contains both private features and common features. The private features of a task are the properties belonging to only this task while the common features are the characteristics shared by all the considered tasks. For TFBS predictions of a TF, the prediction in each cell type can be defined as a task. Thus, TFBS predictions of a TF in multiple cell types form a multi-task learning paradigm.

In multi-task learning, there can be two types of learning methods: the fully shared model and the shared-private model (Liu *et al.*, 2017). The fully shared model uses a single shared CNN to extract features for all cell types, whose hypothesis is that features of individual cell types are shared by all cell types, as illustrated in Figure 1A. The feature space learned by the fully shared model contains common features and also private features of each cell type. Generally speaking, however, TFBSs of a TF in different cell types may have common features and each cell type may also has its own private features, not shared by other cell types. Thus, private features of each cell type will affect the prediction of other cell types. A more serious issue is that, if some cell types contain much more labeled data than others, the feature space learned by the fully shared model may be dominated by private features of these cell types, which will adversely affect the prediction of other cell types with less labeled data, which is counter-productive to the goal of multi-task learning.

The shared-private model, on the other hand, contains a shared CNN to learn common features for all cell types as well a private CNN for each cell type to learn its private features. Features learned for every cell type are separated into two subspace: the common feature space and the private feature space. In the prediction for each cell type, its private features and the common features are integrated as the input. The separation of private features from common features makes sure that the private features of each cell type will not affect the predictions of other cell types. Thus, the shared-private

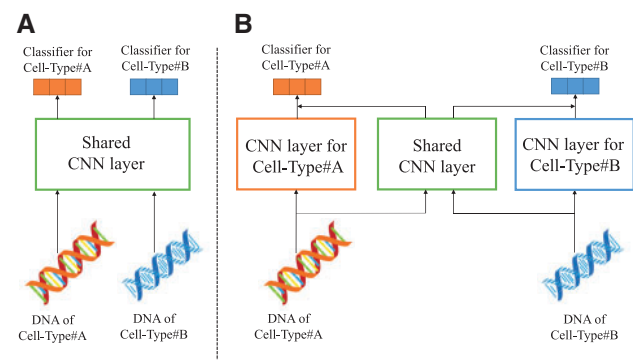


Fig. 1. Architecture of multi-task learning for TFBS prediction. (A) Fully shared method and (B) shared-private method

model can leverage on labeled data available in other cell types to learn solid information from common feature space, especially for cell types with sparse or no labeled data. The shared-private model is illustrated in Figure 1B. Assuming for a TF in a cell type (task)  $m$ , we have a dataset  $D_m$  with  $N_m$  instances, each instance is a pair of a putative TFBS  $x_i^m$  and its corresponding label  $y_i^m$ , that is

$$D_m = \{(x_i^m, y_i^m)\}_{i=1}^{N_m} \quad (3)$$

As CNN is used to learn representations for all putative TFBSs, the private features  $h^m$  and the common features  $s^m$  of a putative TFBS  $x_i^m$  in the cell type  $m$  learned by the shared-private model are formally formulated as:

$$h^m = \text{CNN}(x_i^m, \theta_m) \quad (4)$$

$$s^m = \text{CNN}(x_i^m, \theta_s) \quad (5)$$

where  $\theta_m$  and  $\theta_s$  are the parameters of the private CNN for the cell type  $m$  and the shared CNN, respectively.

Our proposed MTTFSite follows the shared-private model. Thus, MTTFSite has the ability to separate private features of each cell type from common features and can reduce the influence of private features of each cell type to other cell types. In MTTFSite, the network topology of the shared CNN and the private CNN for each cell type contain two parallel CNN models: one is used to learn representations from sequence features and the other is used to learn representations from histone modification features. Then the common features and the private features of each cell type are concatenated to represent instances and fed into a multi-layer perception (MLP) for its prediction.

## 3 Experiments and results

### 3.1 Experimental settings

In MTTFSite, the CNN models in both the shared CNN and private CNNs contain one convolution layer and each convolution layer consists of 200 convolution kernels of length 10. Each convolution layer is followed by a max pooling layer. A dropout regularization layer with dropout probability of 0.5 is used to avoid overfitting. The outputs of the shared CNN and the private CNN for the target cell type are concatenated and inputted into the MLP of the target cell type. The MLP consists of two fully connected layers of 200 neurons and a softmax classifier for predictions. We use Adagrad (Duchi et al., 2011) with a batch size of 64 instances and default learning rate of 0.01. All these hyper-parameters are selected by carrying out experiments on validation set. During training, we train the model for 50 epochs. Once training is finished, we select the model with the highest accuracy on the validation set as our final model and evaluate its performance on the test set. All neural models are implemented in PyTorch.

To evaluate the performance of our proposed MTTFSite for TFBS prediction, we compare MTTFSite with two representative prediction methods: a baseline method and the fully shared model. The baseline method is similar to the DeepBind method proposed by Alipanahi et al. (2015) except that the baseline method also uses histone modification features as additional features. Both the baseline method and the fully shared model contain two parallel CNN models: one is used to learn representations from sequence features and the other to learn representations from histone modification features. The two learned representations are concatenated and fed into an MLP for prediction. The hyperparameters of the baseline method and the fully shared model have the same values as those used in MTTFSite.

### 3.2 Evaluation metrics

AUC, F1-measure and Matthews Correlation Coefficient (MCC) are used as main metrics. AUC is the area under the receiver operating characteristic (ROC) curve. An ROC curve plots the true positive rate (sensitivity) versus the false negative rate (1-specificity) of different thresholds on the importance score. F1-measure is the harmonic average of the precision and recall. Precision is the fraction of true TFBSs among the predicted TFBSs, while recall is the fraction of true TFBSs that have been retrieved over the total amount of TFBSs. MCC is a correlation coefficient between the observed and predicted binary classifications. F1-measure and MCC can be calculated by following formulae:

$$F1 = 2 \times \frac{\text{precision} \times \text{recall}}{\text{precision} + \text{recall}} \quad (6)$$

$$MCC = \frac{TP \times TN - FP \times FN}{\sqrt{(TP + FP)(TP + FN)(TN + FP)(TN + FN)}} \quad (7)$$

where  $TP$ ,  $TN$ ,  $FP$  and  $FN$  denote the number of true positives, the number of true negatives, the number of false positives and the number of false negatives, respectively.

### 3.3 Results of data augmentation using the fully shared model

We first evaluate the performance of the fully shared model on the TFs in the five cell types and compare it with the baseline method. For each TF, the baseline method for each cell type is trained by the training set of this cell type, and is validated and tested by the validation set and the test set of this cell type, respectively. In contrast, the fully shared model of each cell type is trained by the combined training data of all the cell types and is validated and tested by the validation set and the test set of this cell type, respectively.

The comparison between the fully shared model and the baseline method in Supplementary Figure S1A and B shows that the fully shared model performs better than the baseline method for most cell type TF pairs. The box plot in Figure 2 shows that the first quartile, the median and the third quartile of the AUC for the fully shared model are higher than that of the baseline method for all the five cell types. Details of AUC, F1-measure and MCC of the fully shared

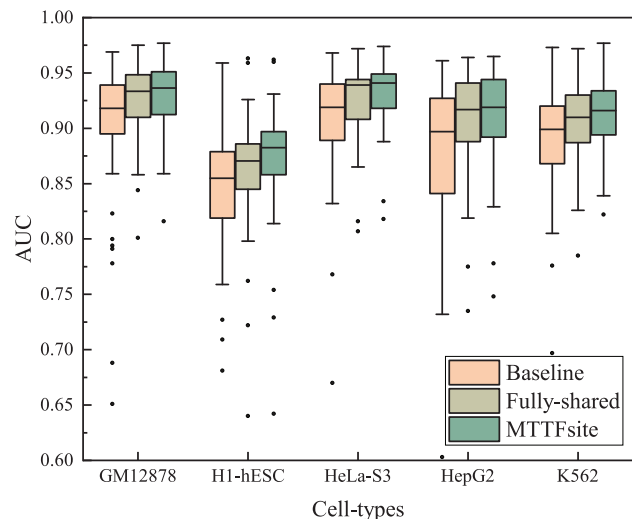


Fig. 2. Box plot depicting the AUC performance of data augmentation by the baseline method, the fully shared model and MTTFSite on TFs in the five cell types

model and the baseline method for each TF of the five cell types are listed in [Supplementary Table S2](#). Results show that the fully shared model outperforms the baseline method for 49 TFs out of the 56 TFs in GM12878, 31 TFs out of the 42 TFs in H1-hESC, 33 TFs out of the 37 TFs in HeLa-S3, 42 TFs out of the 43 TFs in HepG2 and 60 TFs out of the 63 TFs in K562. These are the evidences that multi-task learning can indeed improve the performance of TFBS predictions in most cell type TF pairs through labeled data available in cross-cell types. Thus, we can come to a conclusion that the TFBSs of a TF in multiple different cell types indeed have common features and the common features can be learned by the combined use of the available labeled data from multiple cell types.

### 3.4 Results of data augmentation by MTTFsite

The feature space learned by the fully shared model contains both common features of all the cell types and private features of each cell type. The prediction for each cell type would be influenced by the private features of other cell types as were the case of the fully shared model. Our proposed MTTFsite separates the learning of private features of each cell type from that of the common features. For MTTFsite in data augmentation, each private CNN is trained by the training set of the corresponding cell type while the shared CNN is trained by combined training data of all cell types. In order to evaluate the usefulness of feature separation, we compare the performance of MTTFsite with both the baseline method and the fully shared model.

The comparison among the baseline method, the fully shared model, and our proposed MTTFsite is shown in [Supplementary Figure S1](#). [Supplementary Figure S1B–D](#) show that MTTFsite performs better than both the baseline method and the fully shared model for most cell type TF pairs, although the margin of improvement over the fully shared model is smaller compared with that of the baseline method. The box plot in [Figure 2](#) shows that the first quartile, the median and the third quartile of the AUC for the MTTFsite are higher than that of the fully shared model and the baseline method for all the five cell types. Details of AUC, F1-measure and MCC for the baseline method, the fully shared model, and our proposed MTTFsite for each TF of the five cell types are listed in [Supplementary Table S2](#). [Table 1](#) summarizes the AUC performance gain of MTTFsite compared with the baseline method. For the five cell types, MTTFsite performs better than the baseline method on at least 79.1% TFs of all cell types. The maximum improvement and the average improvement are 12.7 and 2.9% at least, respectively. On average, MTTFsite performs better than the baseline method in more than 92.9% of TFs. The micro average of the maximum improvement and the average improvement are 24.5 and

**Table 1.** Details of the AUC comparison between MTTFsite and the baseline method for data augmentation

Cell type	GM12878	H1-hESC	HeLa-S3	HepG2	K562	Average <sup>a</sup>
Sample total	56	42	37	43	63	48.2
Improvement total	52	37	34	41	60	44.8
Improvement (%)	92.9	88.1	79.1	95.3	95.2	92.9
Maximum <sup>b</sup> (%)	31.7	12.7	22.1	37.8	17.9	24.5
Average <sup>c</sup> (%)	3.6	3.5	3.2	3.8	2.9	3.4

<sup>a</sup>The micro average over the total number of samples.

<sup>b</sup>The maximum improvement.

<sup>c</sup>The average improvement.

3.4%, respectively. The improvements are very significant as shown by  $P$ -value =  $4.71 \times 10^{-37}$  in Wilcoxon signed-ranks test.

[Table 2](#) summarizes the AUC performance gain of MTTFsite compared with the fully shared model. For the five cell types, MTTFsite performs better than the fully shared model in at least 83.9% of TFs for each cell type. The maximum improvement and the average improvement are at least 2.2 and 0.6%, respectively. On average, MTTFsite performs better than the fully shared model significantly in more than 91.7% of TFs with the maximum improvement and the average improvement of 3.1 and 0.8%, respectively ( $P$ -value =  $7.71 \times 10^{-30}$  by Wilcoxon signed-ranks test). Moreover, for some TFs, MTTFsite achieves very promising improvements. For example, the improvements on BCL11A and RXRA in H1-hESC are 2.0 and 2.3%, respectively; the improvements on RAD21 and SMC3 in HeLa-S3 are 2.5 and 2.0%, respectively; the improvements on RAD21 and TR4 in K562 are 2.5 and 3.7%, respectively.

### 3.5 Comparison between MTTFsite and state-of-the-art methods

Recent works with state-of-the-art performance include DNA shape-based method, PWM, DWM as well as deep learning methods. This section will first present comparison of our work with the use of DNA shape features and then proceed to comparison with PWM, DWM and deep learning methods.

DNA shapes represent the 3D structures of DNA. Recently, [Mathelier et al. \(2016a\)](#) proposed four models for TFBS predictions *in vivo* by using DNA shape features including helix twist, minor groove width, propeller twist and the Roll. These four DNA shape features and their corresponding second-order shape features ([Zhou et al., 2015](#)), used to represent putative TFBSs, were computed by DNASHape ([Chiu et al., 2016](#); [Zhou et al., 2013](#)). Four DNASHape-based models we compared with include: (i) one-hot + shape, which combines the one-hot encoding of nucleotides with DNA shape features; (ii) PSSM + shape, which combines PSSM scores with DNA shape features; (iii) TFFM\_d + shape, which combines detailed TFFM scores ([Mathelier and Wasserman, 2013](#)) and DNA shape features, and (iv) TFFM\_f + shape, which combines first-order TFFM scores ([Mathelier and Wasserman, 2013](#)) and DNA shape features. The implementation of the four existing models is all available from the software download webpage (<http://github.com/amathelier/DNASHapedTFBS>). They are implemented in our comparison using their default setup and parameters. In addition to DNASHape, DynaSeq proposed by [Andrabi et al. \(2017\)](#) can also be used to predict DNA shape features. DynaSeq predicts molecular dynamics-derived ensembles of a more exhaustive set of DNA shape features. In this study, we also

**Table 2.** Details of the AUC comparison between MTTFsite and the fully shared model for data augmentation

Cell type	GM12878	H1-hESC	HeLa-S3	HepG2	K562	Average <sup>a</sup>
Sample total	56	42	37	43	63	48.2
Improved total	47	39	37	39	59	44.2
Improvement (%)	83.9	92.9	100	90.7	93.7	91.7
Maximum <sup>b</sup> (%)	2.2	2.8	2.9	2.2	4.7	3.1
Average <sup>c</sup> (%)	0.6	1.2	0.7	0.6	0.8	0.8

<sup>a</sup>The micro average over the total number of samples.

<sup>b</sup>The maximum improvement.

<sup>c</sup>The average improvement.

**Table 3.** The AUC of five state-of-the-art methods and MTTFsite on five TFs in five cell types

TF	Cell type	PWM	DWM	DanQ	DanQ-J	DeepSEA	MTTFsite
CTCF	GM12878	0.586	0.578	<u>0.765</u>	0.731	0.677	<b>0.859</b>
	H1-hESC	0.566	0.575	<u>0.794</u>	0.758	0.689	<b>0.816</b>
	HeLa-S3	0.505	0.509	<u>0.720</u>	0.698	0.670	<b>0.834</b>
	HepG2	0.523	0.527	<u>0.796</u>	0.757	0.697	<b>0.871</b>
	K562	0.923	<b>0.938</b>	0.728	0.693	0.635	<u>0.839</u>
GABP	GM12878	0.844	0.844	0.797	<u>0.845</u>	0.791	<b>0.934</b>
	H1-hESC	0.721	0.740	<u>0.789</u>	<b>0.791</b>	0.763	0.729
	HeLa-S3	<u>0.877</u>	0.875	0.658	0.681	0.630	<b>0.946</b>
	HepG2	0.786	0.791	0.794	<u>0.838</u>	0.795	<b>0.864</b>
	K562	0.756	0.754	0.775	<u>0.793</u>	0.763	<b>0.913</b>
JunD	GM12878	0.906	<u>0.919</u>	0.621	0.606	0.589	<b>0.957</b>
	H1-hESC	0.557	0.566	<u>0.693</u>	0.686	0.643	<b>0.876</b>
	HeLa-S3	<u>0.863</u>	0.860	0.777	0.788	0.711	<b>0.942</b>
	HepG2	<b>0.925</b>	<u>0.878</u>	0.813	0.826	0.738	0.829
	K562	0.684	<u>0.687</u>	0.655	0.653	0.595	<b>0.912</b>
REST	GM12878	0.906	<u>0.919</u>	0.621	0.606	0.589	<b>0.957</b>
	HeLa-S3	0.899	<u>0.922</u>	0.602	0.597	0.559	<b>0.940</b>
	HepG2	0.886	<u>0.902</u>	0.630	0.603	0.602	<b>0.911</b>
	K562	0.867	<u>0.890</u>	0.646	0.645	0.623	<b>0.905</b>
USF2	GM12878	0.891	<u>0.891</u>	0.673	0.698	0.615	<b>0.938</b>
	H1-hESC	0.841	<u>0.851</u>	0.729	0.752	0.662	<b>0.887</b>
	HeLa-S3	0.908	<u>0.912</u>	0.641	0.654	0.561	<b>0.938</b>
	HepG2	0.952	<b>0.953</b>	0.697	0.751	0.591	<u>0.904</u>
	K562	0.921	<u>0.926</u>	0.660	0.715	0.580	<b>0.945</b>

Note: DanQ-J denotes DanQ-JASPAR. The bold and underscore numbers denote the best performer and second best performer, respectively.

compare MTTFsite with DynaSeq. [Supplementary Table S3](#) shows the AUC of MTTFsite, the four DNASHape-based models and DynaSeq on five TFs in the five cell types with a total of 24 cell type TF pairs. Results show that DynaSeq achieves higher AUC than the four DNASHape-based models on 14 cell types TF pairs. It indicates that DNA shape features predicted by DynaSeq are more useful than those predicted by DNASHape, which is consistent with the conclusion drawn in the original publication ([Andrabi et al., 2017](#)). Results also show that our proposed MTTFsite achieves higher AUC than the 4 DNASHape-based models and DynaSeq for 22 cell-type TF pairs. The minimum improvement and the maximum improvement are 2% on GABP in HepG2 and 30% on JunD in GM12878, respectively. The average improvement is 11.6%, which is a very large improvement for TFBS predictions. This first confirms that MTTFsite is more useful than the four DNASHape-based models and DynaSeq for TFBS prediction. One possible reason that MTTFsite outperforms the use of DNA shape features is that DNA shape features are predicted by computational methods from DNA sequences. Thus, there may be redundancy with sequence features. Furthermore, predicted DNA shape features may contain many noises.

Current state-of-the-art methods include PWM ([Stormo, 2000, 2013](#)), DWM ([Siddharthan, 2010](#)) and three deep learning methods: DeepSEA ([Zhou and Troyanskaya, 2015](#)), DanQ ([Quang and Xie, 2016](#)) and DanQ-JASPAR ([Quang and Xie, 2016](#)). PWM and DWM are two useful representation methods for TFBSs and achieved good performance ([Mathelier and Wasserman, 2013](#)). DeepSEA applies CNN and DanQ combines CNN with RNN to learn features for TFBSs. DanQ-JASPAR, an alternative model of DanQ, was developed by initializing half of the kernels in CNN with motifs from the JASPAR database ([Mathelier et al., 2016b](#)). In this evaluation, we implemented PWM and DWM based on Mathelier's work ([Mathelier and Wasserman, 2013](#)). We downloaded DeepSEA from its software's webpage (<http://DeepSEA.princeton.edu/>) and DanQ as well as DanQ-JASPAR from their software's webpage (<http://github.com/uci-cbcl/DanQ>).

Performance data for DeepSEA, DanQ and DanQ-JASPAR are the results of using their default setup and parameters. We compare MTTFsite with these five state-of-the-art methods by 5 TFs in the 5 cell types with a total of 24 cell type TF pairs. As MTTFsite is trained by datasets in five cell types and seven histone marks, we trained DeepSEA, DanQ and DanQ-JASPAR for each TF with the TF binding profiles in the five cell types and the seven histone-mark profiles to make a fair comparison. [Table 3](#) shows the AUC of our proposed MTTFsite and the 5 state-of-the-art methods on the 24 cell type TF pairs. Results show that DWM achieves higher or equal AUC than PWM for 20 cell type TF pairs, which is consistent with the conclusion of the original publication ([Siddharthan, 2010](#)). DanQ achieves higher AUC than DanQ-JASPAR on 12 cell type TF pairs and achieves lower AUC than DanQ-JASPAR on the remaining pairs. This indicates that DanQ and DanQ-JASPAR have comparable performances. DanQ performs better than DeepSEA for most cell type TF pairs, which is consistent with the result reported in the original publication ([Quang and Xie, 2016](#)). Most noticeably, MTTFsite performs better than the 5 state-of-the-art methods in 21 out of the 24 cell type TF pairs. On the 21 pairs, the minimum, the maximum and the average improvement are 0.9, 22.5 and 6.0%, respectively. It should be noted that the performance of DeepSEA, DanQ and DanQ-JASPAR are much better in their reported original publications. However, their performance in this study is much worse. The main reason is that the original models are trained by 690 TF binding profiles for 160 different TFs, 125 DHS profiles as well as 104 histone-mark profiles while the models in this study is trained by TF binding profiles of only 5 cell types and 7 histone-mark profiles. It indicates that the performance of DeepSEA, DanQ and DanQ-JASPAR closely relies on large number of datasets.

### 3.6 Results of cross-cell type prediction by MTTFsite

Due to the high cost of TF ChIP-seq experiments, many cell types only have labeled data for very limited portion of TFs. Most TFs are not labeled. This motivates us to use computational methods to

predict TFBSs for TFs in those cell types that have no labeled data for them. As our proposed MTTFsite can use a shared CNN to learn common features by leveraging on the available labeled data from available cell types, it aims to predict TFBSs for TFs in the cell types without labeled data for them. This is what we refer to as cross-cell type predictions. To evaluate the performance of MTTFsite for cross-cell type TFBS prediction, we assume that only the test set of the target cell type is available while the training set as well as the validation set are unavailable. In cross-cell type prediction, MTTFsite trains both the shared CNN of all cell type and the private CNN of the target cell type by combined training data of cross-cell types. MTTFsite is validated by combined validation set of cross-cell types and then tested on the test set of the target cell type.

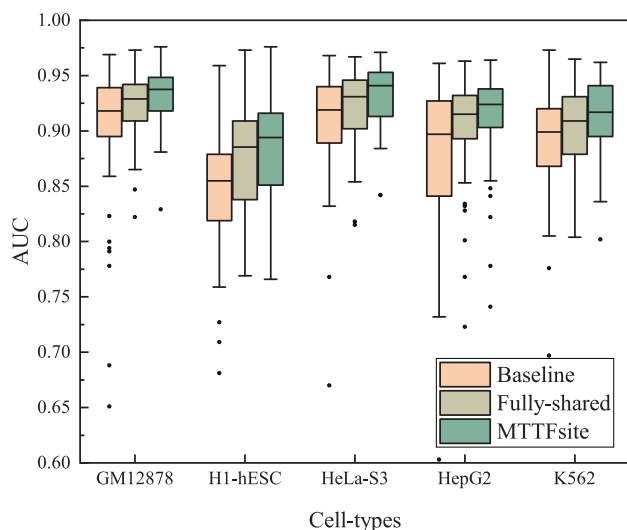


**Fig. 3.** Box plot depicting the AUC performance of cross-cell type prediction by the baseline method, the fully shared model and MTTFsite on TFs in the five cell types

We compare the performance of cross-cell type prediction by MTTFsite with the fully shared model and the baseline method. The fully shared model is trained and validated by cross-cell types like MTTFsite and the baseline method is trained and validated by the target cell type.

The comparison among the baseline method, the fully share model and our proposed MTTFsite is shown in [Supplementary Figure S2](#). [Supplementary Figure S2A](#) and [B](#) show that the fully shared model performs better than the baseline method for most cell type TF pairs. The box plot in [Figure 3](#) shows that the first quartile, the median and the third quartile of the AUC for the fully shared model are higher than that of the baseline method for all the five cell types. It indicates that the use of information of cross-cell types is useful and can achieve better performance than the baseline method which is trained by the target cell type. [Supplementary Figure S2B–D](#) shows that MTTFsite performs better than both the baseline method and the fully shared model for most cell type TF pairs. The box plot in [Figure 3](#) shows that the first quartile, the median and the third quartile of the AUC for MTTFsite are higher than that of both the baseline method and the full-shared model for all the five cell types. Details of AUC, F1-measure and MCC for these three methods on TFs in the five cell types are listed in [Supplementary Table S4](#). [Table 4](#) summarizes the AUC performance gain of MTTFsite compared with the baseline method for cross-cell type TFBS predictions. For the five cell types, MTTFsite outperforms the baseline method on at least 73.8% TFs of each cell type. The maximum improvement and the average improvement are at least 25.7 and at least 5.1%, respectively. On average, MTTFsite outperforms the baseline method in more than 80.9% of TFs. The micro average of the maximum improvement and the average improvement are 36.9 and 5.1%, respectively. The improvement is very significant according to  $P\text{-value} = 1.42 \times 10^{-23}$  by Wilcoxon signed-ranks test.

[Table 5](#) summarizes the AUC performance gain of MTTFsite compared with the fully shared model. For the five cell types, MTTFsite performs better than the fully shared model in at least 88.1% of TFs for each cell type. The maximum improvement and

**Table 4.** Details of the AUC comparison between MTTFsite and the baseline method for cross-cell-type prediction

Cell type	GM12878	H1-hESC	HeLa-S3	HepG2	K562	Average <sup>a</sup>
Sample total	56	42	37	43	63	48.2
Improvement total	46	31	29	35	54	39
Improvement (%)	82.1	73.8	78.4	81.4	85.7	80.9
Maximum <sup>b</sup> (%)	40.9	31.0	25.7	42.0	34.7	36.9
Average <sup>c</sup> (%)	5.1	8.0	4.1	5.1	4.0	5.1

<sup>a</sup>The micro average over the total number of samples.

<sup>b</sup>The maximum improvement.

<sup>c</sup>The average improvement.

**Table 5.** Details of the AUC comparison between MTTFsite and the fully shared model for cross-cell-type prediction

Cell type	GM12878	H1-hESC	HeLa-S3	HepG2	K562	Average <sup>a</sup>
Sample total	56	42	37	43	63	48.2
Improvement total	54	37	36	41	59	45.4
Improvement (%)	96.4	88.1	97.3	95.3	93.7	94.2
Maximum <sup>b</sup> (%)	4.2	3.6	3.5	4.0	4.4	4.0
Average <sup>c</sup> (%)	1.2	1.5	1.2	1.4	1.3	1.3

<sup>a</sup>The micro average over the total number of samples.

<sup>b</sup>The maximum improvement.

<sup>c</sup>The average improvement.

the average improvement are at least 3.5 and at least 1.2%, respectively. On average, MTTFSite performs better than the fully shared model significantly in more than 94.2% of TFs with the maximum improvement and the average improvement of 4.0 and 1.3%, respectively ( $P$ -value =  $4.55 \times 10^{-13}$  by Wilcoxon signed-ranks test). The improvements for many TFs are quite promising. For example, the improvements for RAD21 and MAFK in H1-hESC and CTCF, RAD21 and SMC3 in K562 are more than 3.0%; the improvements for CTCF and EZH2 in GM12878, CTCF in HeLa-S3, NRSF in HepG2 are more than 4.0%. It is a strong indication that MTTFSite has a better prediction power than that of the fully shared model.

By comparing MTTFSite with the full-shared model, we find that the private CNNs of the cell types without labeled data in MTTFSite function similarly to the shared CNN in the fully shared model because they both are trained by the combined training data from cross-cell types. The only difference is that MTTFSite contains both features learned by private CNNs and by the shared CNN whereas the fully shared model only uses features learned by the shared CNN. In the fully shared model, if some cell types contain too much training data, the learned features are dominated by private features of these cell types such that many common features are lost. As MTTFSite can separate private features from common features, the lost common features in the private CNNs can be complemented by the common features learned by the shared CNN. Therefore, the features learned by MTTFSite for each cell type contain more common features than that learned by the fully shared model.

In order to further demonstrate the performance of MTTFSite for cross-cell type prediction, we evaluate MTTFSite on TFs in K562 cells from PIQ study (Sherwood et al., 2014), which are available from online resource located at <http://piq.csail.mit.edu/data/141105-3618f89-hg19k562.calls/141105-3618f89-hg19k562.calls.tar.gz>. Although there are a total of 1316 TFs with genome-wide TFBSs available in K562 from PIQ study, only 28 TFs have training set in at least one cell type of the 5 cell types in this study except K562. So MTTFSite is only tested on the 28 TFs with available training data. In Andrabi's work (Andrabi et al., 2017), TFBSs are selected from the 'calls' data and equal number of non-TFBSs are selected with the cutoff score of 0.25, where the maximum number of TFBSs and non-TFBSs was fixed at 2000 by random sampling. However, in order to evaluate MTTFSite on genome scale, we collected all the TFBSs from the 'calls' data and equal number of non-TFBSs to make up test set. Thus, for each TF, MTTFSite is trained by the combined training data available in the four cell types in this study and tested on the test set from PIQ study. The performance is listed in Supplementary Table S5. Results show that MTTFSite achieves good performance on most TFs and the AUC performance on seven TFs is more than 0.8. As training data comes from ChIP-Seq while testing data comes from DNase-Seq, results indicate that MTTFSite can be applied for cross-platform prediction.

ENCODE-DREAM *in vivo* transcription factor binding challenge contains a across-cell type prediction challenge, in which each TF has cell types for training and held-out cell types for testing. We downloaded the 13 cell type TF pairs in the Final Submission Round. For each TF, MTTFSite is trained by at least one cell type and tested by held-out cell types, which are newly generated and have never been previously released by ENCODE. As the challenge do not provide histone modification features, MTTFSite is trained only from DNA sequences and chromatin accessibility measured by DNase-Seq. The advantage of MTTFSite is that it can learn common features in histone modification features for TFBSs shared by multiple cell types. Even though, MTTFSite trained from DNA sequence and chromatin accessibility cannot fully demonstrate the

advantages of our method, MTTFSite still achieves very good performance on the 13 cell type TF pairs. The performance is listed in Supplementary Table S6. Supplementary Table S6 shows that MTTFSite achieves good performance for all the 13 cell type TF pairs. Specifically, AUC of all the 13 pairs is more than 0.9 and AUC of 7 pairs is even more than 0.95. Results indicate that MTTFSite can achieve good performance for cross-cell type TFBS prediction even when histone modification features are not available.

### 3.7 Results on cell type shared TFBS and cell-type-specific TFBS

One advantage of MTTFSite is that it can leverage on cell type shared TFBSs available in other cell types to train the shared CNN. To validate this, we evaluate the performance of MTTFSite on cell type shared TFBSs and cell-type-specific TFBSs, separately. In this study, cell type shared TFBSs of a cell type are defined as the TFBSs which have at least a TFBS of other cell types in its range of 100 bp. The remaining TFBSs are referred to as cell-type-specific TFBSs. According this criterion, TFBSs of each cell type are divided into cell type shared TFBSs and cell-type-specific TFBSs. Details of the number of cell type shared TFBSs and cell-type-specific TFBSs for TFs in the five cell types is listed in Supplementary Table S7. For each target cell type, MTTFSite is trained by combined labeled data available in cross-cell types and tested on cell type shared TFBSs and cell-type-specific TFBSs of the target cell type, separately. Sensitivity is used to evaluate the performance of MTTFSite. The sensitivity of MTTFSite for TFs in the five cell types is listed in Figure 4. Figure 4A shows that MTTFSite achieves higher sensitivity on cell type shared TFBSs than cell-type-specific TFBSs for all cell type TF pairs except one. Figure 4B shows that the first quartile, the median and the third quartile of the sensitivity for cell type shared TFBSs are higher than that for cell-type-specific TFBSs for TFs in all the five cell types. Details of the sensitivity for cell type shared and specific TFBSs for TFs in the five cell types are listed as Supplementary Table S8. Results indicate that MTTFSite indeed can effectively leverage on cell type shared TFBSs available in cross-cell types to learn common features of all cell types.

As MTTFSite achieves higher sensitivity on shared TFBSs than specific TFBSs in almost all the five cell types for each TF, the shared TFBSs dominate the performance of MTTFSite. If other cell types have more shared TFBSs available by target cell types, MTTFSite can achieve higher prediction performance. Therefore, high-quality predictions of MTTFSite for each TF rely on available TFBSs shared by target cell types and other cell types.

It should also be noted that Figure 4B shows that specific TFBSs in H1-hESC achieve the lowest sensitivity among the five cell types. It is possible that MTTFSite achieves low sensitivity scores for specific TFBSs in H1-hESC because specific TFBSs in H1-hESC have different characteristics compared with other cell types for some TFs. Based on this hypothesis, we conducted an additional experiment to calculate the cosine similarities among the five cell types for both specific TFBSs and shared TFBSs of each TF. For each TF, we first represent specific TFBSs and shared TFBSs by histone modification features and calculate their center in each cell type by calculating the median value of each histone modification feature. Then, based on these centers, we calculate the cosine similarity between any two cell types. Finally, for each cell type, its cosine similarities to other cell types are averaged. The average cosine similarities of the five cell types for both specific TFBSs and shared TFBSs of each TF are shown in Figure 5. The figure shows that the cosine



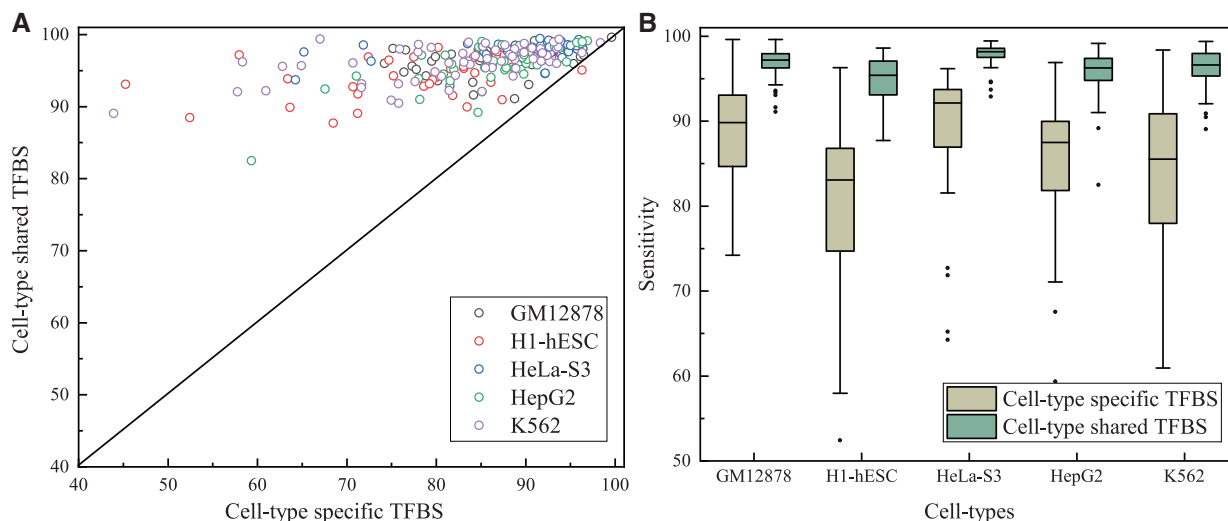


**Fig. 4.** (A) Scatter plot depicting the distribution of the AUC performance for cell type shared TFBSs and cell-type-specific TFBSs. (B) Box plot depicting the AUC performance for cell type shared TFBSs and cell-type-specific TFBSs on TFs in the five cell types

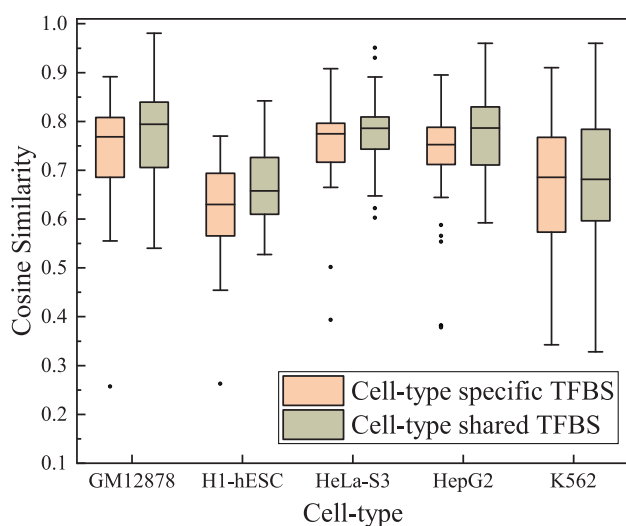


**Fig. 5.** Cosine similarities of cell-type-specific TFBSs in different cell types

similarities of shared TFBSs are higher than that of specific TFBSs in the five cell types. This explains why MTTFSite achieves higher performance for shared TFBSs than that for specific TFBSs. Figure 5 also shows that specific TFBSs in H1-hESC have the lowest cosine similarity to other cell types among the five cell types. This is indeed likely the reason that specific TFBSs in H1-hESC achieve the lowest sensitivity. Figure 5 further shows that K562 has lower cosine similarity than the other three cell types. This explains why specific TFBSs in K562 achieve lower sensitivity than the other three cell types. The other three cell types have small cosine similarity differences, so their specific TFBSs have small sensitivity differences.

nextPBM has been proposed to characterize the impact of cofactors and phosphorylation on TF binding and determine cell-type-specific TFBSs (Mohaghegh *et al.*, 2019). The authors analyzed DNA binding of PU.1/SPI1 and IRF8 from human monocytes and found that cofactors and phosphorylation have no effect on autonomous PU.1/SPI1 binding and only have effect on its cooperative binding with monocyte-specific cofactors. Thus, nextPBMs can only identify cell type specific cooperative TFBSs of PU.1/SPI1 with IRF8. As our proposed MTTFSite needs cell type specific TFBSs to learn

cell-type-specific features by private CNNs and PU.1/SPI1 does not have cell-type-specific TFBSs, current datasets used by nextPBM are inappropriate to improve MTTFSite. Nevertheless, nextPBM is capable of identifying cell-type-specific TFBSs by comparing TFBSs from nuclear extracts to that from *in vitro* transcription/translation protein. Therefore, in the future, we can apply nextPBM to identify cell-type-specific TFBSs for TFs. This should help to improve MTTFSite for cell-type-specific TFBS prediction by learning cell-type-specific features through private CNNs using the identified cell-specific TFBSs identified by nextPBM.

### 3.8 Application in gene expression prediction

TFs can bind to DNA through TFBSs to regulate gene expression. Therefore, we hypothesize that TFBSs are significant for gene expression regulations and can play an important role in gene expression prediction.

In this work, we propose a new gene expression prediction method, referred to as *TFChrom*, by combining the use of TFBSs predicted by MTTFSite and histone modification features. We evaluate *TFChrom* by 20 cell types from the Roadmap Epigenomics Consortium (RMEC) (Kundaje *et al.*, 2015). These 20 cell types have seven common histone modification features (Boyle *et al.*, 2008; Crawford *et al.*, 2005). Since these 20 cell types do not have available labeled data for any TF, MTTFSite combines the available labeled data from GM12878, H1-hESC, HeLa-S3, HepG2 and K562 as training data to predict TFBSs for TFs in these 20 cell types. More specifically, we predict the TFBSs for 72 TFs in the 20 cell types, which are listed in Supplementary Table S1. As the 20 cell types from RMEC and the 5 cell types with labeled data contain seven common histone modification features including *H3K27ac*, *H3K37me3*, *H3K36me3*, *H3K9ac*, *H3K9me3*, *H3K4me1* and *H3K4me3*, these seven histone modification features are used in both the TFBS prediction and the gene expression prediction. Details of the definition of gene expression prediction and the used gene encoding method are given in Supplementary Methods.

To consider the relative importance of predicted TFBSs and histone modification features, we use two baseline methods for comparison: (i) using only predicted TFBSs and (ii) using only histone modification features. our proposed *TFChrom* combines both the predicted TFBSs and histone modification features. Table 6 gives the

**Table 6.** The AUC of the gene expression predictions on the 20 cell types from RMEC

Cells	TFBS	Histone	Combine
Breast_vHMEC	0.779	<u>0.859</u>	<b>0.864</b>
Fetal_Brain	0.764	<u>0.848</u>	<b>0.855</b>
Fetal_Muscle_Leg	0.773	<u>0.854</u>	<b>0.858</b>
Fetal_Muscle_Trunk	0.759	<u>0.802</u>	<b>0.849</b>
Gastric	0.752	<u>0.813</u>	<b>0.819</b>
H1_BMP4_Derived_Mesendoderm_Cultured_Cells	0.746	<u>0.787</u>	<b>0.827</b>
H1_BMP4_Derived_Trophoblast_Cultured_Cells	0.751	<u>0.831</u>	<b>0.840</b>
H1_Cell_Line	0.754	<u>0.837</u>	<b>0.844</b>
H1_Derived_Mesenchymal_Stem_Cells	0.782	<u>0.833</u>	<b>0.839</b>
H1_Derived_Neuronal_Progenitor_Cultured_Cells	0.752	<u>0.833</u>	<b>0.839</b>
IMR90_Cell_Line	0.789	<u>0.852</u>	<b>0.860</b>
iPS_DF_19.11_Cell_Line	0.744	<u>0.808</u>	<b>0.813</b>
iPS_DF_6.9_Cell_Line	0.746	<u>0.823</u>	<b>0.826</b>
Mobilized_CD34_Primary_Cells	0.797	<u>0.872</u>	<b>0.878</b>
Pancreas	0.754	<u>0.824</u>	<b>0.832</b>
Penis_Foreskin_Fibroblast_Primary_Cells	0.815	<u>0.885</u>	<b>0.891</b>
Penis_Foreskin_Keratinocyte_Primary_Cells	0.794	<u>0.872</u>	<b>0.880</b>
Penis_Foreskin_Melanocyte_Primary_Cells	0.801	<u>0.875</u>	<b>0.881</b>
Psoas_Muscle	0.767	<u>0.801</u>	<b>0.858</b>
Small_Intestine	0.767	<u>0.835</u>	<b>0.840</b>

Note: The bold and underscore numbers denote the best performer and second best performer, respectively.

performance evaluation of the three methods. Note that the maximum, the minimum and the average AUC of prediction using only predicted TFBSs are 0.815, 0.744 and 0.769, far better than random guessing. This is a strong indication that our hypothesis is correct that TFBSs indeed play an important role in gene expression predictions.

Table 6 also shows that TFChrom outperforms the method using only histone modification features. The Wilcoxon signed-ranks test with  $P$ -value of at least  $3.36e-5$  also indicates that the improvement is very significant. For some cell types, the performance improvement by TFChrom is quite prominent. For example, for Fetal\_Muscle\_Trunk, H1\_BMP4\_Derived\_Trophoblast\_Cultured\_Cells and Psoas\_Muscle, the improve in AUC are 3.3, 4.0 and 5.7%, respectively. These are evidences that TFBSs predicted by our proposed MTTFSite and histone modification features are complementary for gene expression predictions.

Several computational methods were proposed for gene expression predictions. TEPIIC (Schmidt et al., 2017), Zhang's method (Zhang and Li, 2017) and DeepChrom (Singh et al., 2016) are three methods with state-of-the-art performance. As the used datasets and the definition for the problem of gene expression prediction in TFChrom are different from TEPIIC and Zhang's method, we only compare TFChrom with DeepChrom. DeepChrom, proposed by Singh et al. (2016), uses CNN and histone modification features, which outperforms most previous methods. As TFChrom has 15 cell types common with DeepChrom, we compare them on those 15 cell types. Supplementary Table S9 shows the performance comparison of TFChrom and DeepChrom. Note that the AUC of DeepChrom on the 15 common cell types are given directly from Singh's work. Supplementary Table S9 shows that our proposed TFChrom performs far better than DeepChrom on 14 out of the 15 common cell types. The maximum, the minimum and the average improvement in AUC is 12, 1.7 and 6.2%, respectively, which are quite large. As both methods use the histone modification features, the main difference is that TFChrom also use the additional feature from the predicted TFBSs. Thus, it is fair to say that the improvement is contributed by the predicted TFBSs using MTTFSite.

## 4 Conclusion

In this paper, we present a novel data augmentation method using multi-task learning framework, MTTFSite, for TFBS predictions. MTTFSite contains a shared CNN to learn common features of all cell types and a private CNN for each cell type to learn private features. The aim of the algorithm is to make use of common features cross different cell types to help predicting TFBSs for TFs in cell types that have no labeled data. Performance evaluation shows MTTFSite can effectively leverage on labeled data available in cross-cell types to learn common features of all cell types. As MTTFSite can separate private features from common features, it outperforms the fully shared model significantly. For cross-cell-type prediction, MTTFSite also outperforms the compared models. This is a clear indication that common features learned by MTTFSite from labeled data available in cross-cell types are indeed useful for cross-cell-type predictions. To further prove the usefulness of MTTFSite, we propose to make use of the predicted TFBSs for gene expression prediction. The new gene expression prediction method TFChrom makes combined use of the TFBSs predicted by MTTFSite and histone modification features. The evaluation on 20 cell types shows that TFBSs predicted by MTTFSite significantly improves the performance of gene expression predictions compared with the state-of-the-art methods. Gene expressions of organisms are closely related to identification of diseases. For example, low expression of BRCA1 plays an important role in breast and ovarian cancers. Therefore, accurate gene expressions predicted by our proposed TFChrom can provide valuable reference and assistance for the diagnosis and treatment of dozens of diseases.

One direction of future works is to investigate the relative importance of labeled data from different cell types in cross-cell type TFBS prediction. The second direction is to investigate the prediction of TFs of cell types without any labeled data by using labeled data of other TFs from the same cell type, which is also referred to as cross-TF TFBS predictions.

## Funding

This work was supported by the National Natural Science Foundation of China U1636103, 61632011, 61876053, Shenzhen Foundational Research Funding JCYJ20170307150024907, JCYJ2018057183527919, Key Technologies

Research and Development Program of Shenzhen JSGG20170817140856618 and H-2020 (no. 794196).

*Conflict of Interest:* none declared.

## References

- Alipanahi, B. *et al.* (2015) Predicting the sequence specificities of DNA- and RNA-binding proteins by deep learning. *Nat. Biotechnol.*, **33**, 831–838.
- Andrabi, M. *et al.* (2017) Predicting conformational ensembles and genome-wide transcription factor binding sites from DNA sequences. *Sci. Rep.*, **7**, 4071.
- Barash, Y. *et al.* (2003) Modeling dependencies in protein-DNA binding sites. In: *Proceedings of the Seventh Annual International Conference on Research in Computational Molecular Biology*, pp. 28–37. ACM, New York, NY.
- Berger, M.F. *et al.* (2006) Compact, universal DNA microarrays to comprehensively determine transcription-factor binding site specificities. *Nat. Biotechnol.*, **24**, 1429–1435.
- Boyle, A.P. *et al.* (2008) High-resolution mapping and characterization of open chromatin across the genome. *Cell*, **132**, 311–322.
- Breiman, L. (2001) Random forests. *Mach. Learn.*, **45**, 5–32.
- Bryne, J.C. *et al.* (2007) JASPAR, the open access database of transcription factor-binding profiles: new content and tools in the 2008 update. *Nucleic Acids Res.*, **36**, D102–D106.
- Bulyk, M.L. (2003) Computational prediction of transcription-factor binding site locations. *Genome Biol.*, **5**, 201.
- Bulyk, M.L. *et al.* (2002) Nucleotides of transcription factor binding sites exert interdependent effects on the binding affinities of transcription factors. *Nucleic Acids Res.*, **30**, 1255–1261.
- Chiu, T.P. *et al.* (2016) DNashapeR: an R/Bioconductor package for DNA shape prediction and feature encoding. *Bioinformatics*, **32**, 1211.
- Crawford, G.E. *et al.* (2005) Genome-wide mapping of DNase hypersensitive sites using massively parallel signature sequencing MPSS. *Genome Res.*, **16**, 123.
- Dror, I. *et al.* (2016) How motif environment influences transcription factor search dynamics: finding a needle in a haystack. *BioEssays*, **38**, 605–612.
- Duchi, J. *et al.* (2011) Adaptive subgradient methods for online learning and stochastic optimization. *J. Mach. Learn. Res.*, **12**, 257–269.
- ENCODE Project Consortium. (2004) The ENCODE (ENCyclopedia Of DNA Elements) Project. *Science*, **306**, 636–640.
- Harbison, C.T. *et al.* (2004) Transcriptional regulatory code of a eukaryotic genome. *Nature*, **431**, 99–104.
- Holloway, D.T. *et al.* (2005) Integrating genomic data to predict transcription factor binding. *Genome Inform.*, **16**, 83–94.
- Iyer, V.R. *et al.* (2001) Genomic binding sites of the yeast cell-cycle transcription factors SBF and MBF. *Nature*, **409**, 533–538.
- Kim, T.H. *et al.* (2005) A high-resolution map of active promoters in the human genome. *Nature*, **436**, 876–880.
- Kumar, S. and Bucher, P. (2016) Predicting transcription factor site occupancy using DNA sequence intrinsic and cell-type specific chromatin features. *BMC Bioinformatics*, **17**, S4.
- Kundaje, A. *et al.* (2015) Integrative analysis of 111 reference human epigenomes. *Nature*, **518**, 317–330.
- Lenhard, B. *et al.* (2003) Identification of conserved regulatory elements by comparative genome analysis. *J. Biol.*, **2**, 13.
- Liu, P. *et al.* (2017) Adversarial multi-task learning for text classification. In: *Proceedings of the 55th Annual Meeting of the Association for Computational Linguistics*, pp. 1–10. Association for Computational Linguistics, Vancouver, Canada.
- Luscombe, N.M. *et al.* (2001) Amino acid–base interactions: a three-dimensional analysis of protein–DNA interactions at an atomic level. *Nucleic Acids Res.*, **29**, 2860–2874.
- Man, T.-K. and Stormo, G.D. (2001) Non-independence of Mnt repressor–operator interaction determined by a new quantitative multiple fluorescence relative affinity (QuMFRA) assay. *Nucleic Acids Res.*, **29**, 2471–2478.
- Marinescu, V.D. *et al.* (2004) The mapper database: a multi-genome catalog of putative transcription factor binding sites. *Nucleic Acids Res.*, **33**, D91–D97.
- Mathelier, A. and Wasserman, W.W. (2013) The next generation of transcription factor binding site prediction. *PLoS Comput. Biol.*, **9**, e1003214.
- Mathelier, A. *et al.* (2016a) DNA shape features improve transcription factor binding site predictions in vivo. *Cell Syst.*, **3**, 278–286.
- Mathelier, A. *et al.* (2016b) JASPAR 2016: a major expansion and update of the open-access database of transcription factor binding profiles. *Nucleic Acids Res.*, **44**, D110–D115.
- Matys, V. *et al.* (2006) TRANSFAC<sup>®</sup> and its module TRANSCompel<sup>®</sup>: transcriptional gene regulation in eukaryotes. *Nucleic Acids Res.*, **34**, D108–D110.
- Mohaghegh, N. *et al.* (2019) Nextpbm: a platform to study cell-specific transcription factor binding and cooperativity. *Nucleic Acids Res.*, **47**, e31.
- Quang, D. and Xie, X. (2016) DanQ: a hybrid convolutional and recurrent deep neural network for quantifying the function of DNA sequences. *Nucleic Acids Res.*, **44**, e107.
- Ren, B. *et al.* (2000) Genome-wide location and function of DNA binding proteins. *Science*, **290**, 2306–2309.
- Schmidt, F. *et al.* (2017) Combining transcription factor binding affinities with open-chromatin data for accurate gene expression prediction. *Nucleic Acids Res.*, **45**, 54–66.
- Sherwood, R.I. *et al.* (2014) Discovery of directional and nondirectional pioneer transcription factors by modeling DNase profile magnitude and shape. *Nat. Biotechnol.*, **32**, 171–178.
- Siddharthan, R. (2010) Dinucleotide weight matrices for predicting transcription factor binding sites: generalizing the position weight matrix. *PLoS One*, **5**, e9722.
- Singh, R. *et al.* (2016) DeepChrome: deep-learning for predicting gene expression from histone modifications. *Bioinformatics*, **32**, i639–i648.
- Stormo, G.D. (2000) DNA binding sites: representation and discovery. *Bioinformatics*, **16**, 16–23.
- Stormo, G.D. (2013) Modeling the specificity of protein-DNA interactions. *Quant. Biol.*, **1**, 115.
- Tomovic, A. and Oakeley, E.J. (2007) Position dependencies in transcription factor binding sites. *Bioinformatics*, **23**, 933–941.
- Tsai, Z.T.-Y. *et al.* (2015) Contribution of sequence motif, chromatin state, and DNA structure features to predictive models of transcription factor binding in yeast. *PLoS Comput. Biol.*, **11**, e1004418.
- Wang, S. *et al.* (2016) Protein secondary structure prediction using deep convolutional neural networks. *Scientific Rep.*, **6**, 18962.
- Wasserman, W.W. and Sandelin, A. (2004) Applied bioinformatics for the identification of regulatory elements. *Nat. Rev. Genet.*, **5**, 276–287.
- Won, K.-J. *et al.* (2010) Genome-wide prediction of transcription factor binding sites using an integrated model. *Genome Biol.*, **11**, R7.
- Zambelli, F. *et al.* (2013) Motif discovery and transcription factor binding sites before and after the next-generation sequencing era. *Brief. Bioinform.*, **14**, 225–237.
- Zeng, H. *et al.* (2016) Convolutional neural network architectures for predicting DNA-protein binding. *Bioinformatics*, **32**, i121–i127.
- Zhang, L.Q. and Li, Q.Z. (2017) Estimating the effects of transcription factors binding and histone modifications on gene expression levels in human cells. *Oncotarget*, **8**, 40090–40103.
- Zhou, J. and Troyanskaya, O.G. (2015) Predicting effects of noncoding variants with deep learning-based sequence model. *Nat. Methods*, **12**, 931–934.
- Zhou, Q. and Liu, J.S. (2004) Modeling within-motif dependence for transcription factor binding site predictions. *Bioinformatics*, **20**, 909–916.
- Zhou, T. *et al.* (2013) DNashape: a method for the high-throughput prediction of DNA structural features on a genomic scale. *Nucleic Acids Res.*, **41**, W56–W62.
- Zhou, T. *et al.* (2015) Quantitative modeling of transcription factor binding specificities using DNA shape. *Proc. Natl. Acad. Sci.*, **112**, 4654–4659.